Please cite this article in press as: Acharya et al., The Effect of (−)-Epigallocatechin-3-Gallate on the Amyloid-β Secondary Structure, Biophysical Journal (2020), https://doi.org/10.1016/j.bpj.2020.05.033

Biophysical *Journal*
Article

Biophysical Society

The Effect of (−)-Epigallocatechin-3-Gallate on the Amyloid-β Secondary Structure

Atanu Acharya,[1,2] Julia Stockmann,[3,4] Léon Beyer,[3,4] Till Rudack,[3,4] Andreas Nabers,[3,4,*] James C. Gumbart,[1,2] Klaus Gerwert,[3,4,*] and Victor S. Batista[5,*]

[1]School of Physics and [2]School of Chemistry and Biochemistry, Georgia Institute of Technology, Atlanta, Georgia; [3]Biospectroscopy, Center for Protein Diagnostics and [4]Department of Biophysics, Ruhr University Bochum, Bochum, Germany; and [5]Department of Chemistry, Yale University, New Haven, Connecticut

ABSTRACT Amyloid-β (Aβ) is a macromolecular structure of great interest because its misfolding and aggregation, along with changes in the secondary structure, have been correlated with its toxicity in various neurodegenerative diseases. Small drug-like molecules can modulate the amyloid secondary structure and therefore have raised significant interest in applications to active and passive therapies targeting amyloids. In this study, we investigate the interactions of epigallocatechin-3-gallate (EGCG), found in green tea, with Aβ polypeptides, using a combination of in vitro immuno-infrared sensor measurements, docking, molecular dynamics simulations, and ab initio calculations. We find that the interactions of EGCG are dominated by only a few residues in the fibrils, including hydrophobic π-π interactions with aromatic rings of side chains and hydrophilic interactions with the backbone of Aβ, as confirmed by extended (1-μs-long) molecular dynamics simulations. Immuno-infrared sensor data are consistent with degradation of Aβ fibril induced by EGCG and inhibition of Aβ fibril and oligomer formation, as manifested by the recovery of the amide-I band of monomeric Aβ, which is red-shifted by 26 cm^{-1} when compared to the amide-I band of the fibrillar form. The shift is rationalized by computations of the infrared spectra of Aβ42 model structures, suggesting that the conformational change involves interchain hydrogen bonds in the amyloid fibrils that are broken upon binding of EGCG.

SIGNIFICANCE Inhibition of fibril formation or degradation of amyloid-β (Aβ) deposits by small drug-like molecules has great potential for passive or active therapies of Alzheimer's disease. Databases comprised of a very large number of molecules can be tested as potential drugs targeting amyloids. In this context, understanding interactions between these molecules and Aβ are extremely important. We investigate the disruptive effect of EGCG, a natural molecule found in green tea, on the secondary structure of Aβ polypeptides combining extended molecular dynamics simulation, ab initio calculations, and in vitro immuno-infrared analyses. Beyond EGCG, the reported characterization of drug docking effects can significantly reduce the number of candidates to be tested in clinical trials, leading to reduced expenses.

INTRODUCTION

Protein aggregation plays a significant role in various neurodegenerative diseases, including Alzheimer's and Parkinson's diseases. These common types of dementia cost more than $277 billion in 2018 and are estimated to reach $1.1 trillion by the year 2050 (1). Currently, there is no cure for either one of these diseases. Available drugs alleviate symptoms but do not halt the slow deterioration of the brain. Plaques formed by the deposition of amyloid-β (Aβ) aggregates are associated with the Alzheimer's disease pathology (2,3). Remarkably, in its monomeric form, Aβ is soluble and nontoxic for cells. Conversion of Aβ into insoluble aggregates and pathogenic Aβ fibrils is mediated by rapid self-assembly and formation of oligomers (4–9) that are further aggregated and deposited as plaques (8,10). Recently, Aβ oligomers were found to be toxic variants, which cause severe damage in the synaptic neurotransmission and neuron death (11,12). Moreover, fibrils and oligomers are thought to cause lipid bilayer disruption, inflammation, lipid peroxidation, and production of reactive oxygen species (11,13–15). Structural studies reveal that Aβ fibrils and oligomers predominantly consist of β-sheets in a cross-β conformation (11,16). The β-sheet-enriched structures (100%) of amyloids are more conducive to

Submitted October 28, 2019, and accepted for publication May 4, 2020.

*Correspondence: andreas.nabers@rub.de or gerwert@bph.rub.de or victor.batista@yale.edu

Editor: Heping Cheng.

https://doi.org/10.1016/j.bpj.2020.05.033

Please cite this article in press as: Acharya et al., The Effect of (−)-Epigallocatechin-3-Gallate on the Amyloid-β Secondary Structure, Biophysical Journal (2020), https://doi.org/10.1016/j.bpj.2020.05.033

oligomerization than structures with much lower β-sheet content (17). Therefore, their toxicity could be reduced by preventing the β-sheet-enriched fibril formation or by inducing degradation of already formed β-sheet-based aggregates.

Several naturally occurring polyphenolic molecules have been identified as anti-amyloidogenic (8,18–25) because they prevent Aβ fibril formation. For example, resveratrol (found in grapes and red wine) is known to significantly lower the level of secreted and intracellular Aβ (19,22). A small number of nonphenolic (26) and small-peptide (27) inhibitors were also identified. Herein, we focus on epigallocatechin-3-gallate (EGCG), a small molecule found in green tea, which is the most notable phenolic amyloid inhibitor (18). Although EGCG has been proposed to prevent fibril formation and induce degradation of the previously formed fibril structures of α-synuclein and Aβ (23,24), the type of interactions between EGCG and the Aβ fibril responsible for structural disruption remain unknown, preventing the rational design of more effective inhibitors informed by the EGCG lead molecule. The effects of small molecules on the secondary structure of Aβ can be explored by infrared (IR) spectroscopy because secondary structures of Aβ can be differentiated by the vibrational frequencies of the carbonyl stretching (amide-I) modes. Therefore, the oligomerization of Aβ is directly reflected in its amide-I maxima. In this study, we explore the effect of EGCG on the vibrational properties of Aβ. Although the actual dynamics of the corresponding structural rearrangement induced by EGCG could not be captured even with a nearly 1-μs molecular dynamics (MD) trajectory (28,29), those MD simulations were indicative of the inhibitory capabilities of EGCG toward fibrillation and oligomerization (29).

Here, we apply a combination of experimental and theoretical methods to characterize first the spectral signatures of structural rearrangements due to β-sheet-enriched Aβ degradation or EGCG-induced inhibition of Aβ fibril formation. The measurements are performed using the immuno-infrared sensor based on attenuated total reflection Fourier transform infrared spectroscopy (ATR-FTIR) technique. That sensor can monitor the effects of therapeutic molecules on disease-related biomarkers in a label-free manner as shown for methylene blue, Congo red, and berberine on Aβ and τ from human body fluids in real time under physiological conditions (30–33). We then investigate the interactions between the Aβ fibril model and EGCG using docking calculations, followed by MD simulations of the docked complex. Finally, we compute the IR spectra of model dimers (fibril and nonfibril models) and monomers of Aβ to rationalize the EGCG-induced spectral shift obtained in our experiments. Our calculations are based on an ab initio divide-and-conquer methodology, previously introduced in the computation of sum-frequency generation spectra (34,35). We focus exclusively on the effects of EGCG on $A\beta_{42}$ fibrils because $A\beta_{42}$ is more toxic than $A\beta_{40}$.

MATERIALS AND METHODS

Experimental details

Chemicals and solutions were purchased from Sigma-Aldrich (Hamburg, Germany). All antibodies were obtained from NanoTools (Teningen, Germany). Functionalization of the activated sensor surface followed the procedures reported in our previous work (30–33).

Preparation of Aβ monomers

Synthetic $A\beta_{42}$ (Bachem, Bubendorf, Switzerland) was dissolved in hexafluoroisopropanol at a concentration of 2 mg/mL overnight at room temperature to obtain a monomeric stock. We then dispensed this stock to 100-μg aliquots, followed by evaporation for 15 min in a speed vac (Concentrator Plus; Eppendorf, Hamburg, Germany) and 45 min in vacuum. For monomeric $A\beta_{42}$, the peptide film was dissolved in phosphate buffer (137 mM NaCl, 2.7 mM KCl, 10 mM Na_2HPO_4, 2 mM NaH_2PO_4) and immediately used for infrared analysis.

Preparation of Aβ fibrils

For fibrillation, the $A\beta_{42}$ peptide film was dissolved in phosphate buffer (137 mM NaCl, 2.7 mM KCl, 10 mM Na_2HPO_4, 2 mM NaH_2PO_4) and shaken (Heidolph, Schwabach, Germany) (optional: treated with ultrasonic) until the film was in solution. Afterwards, the peptide solution was incubated for at least 24 h at 37°C and 350 rpm (Thermomixer Comfort; Eppendorf). Fibrils were centrifuged for 30 min at 13,000 × *g*. After discarding the supernatant, the pellet was gently resuspended in a buffer. We determined the concentration of denatured peptides by ultraviolet spectrometer at 280 nm.

FTIR measurements

A vertical variable angle ATR setup (Specac, London, UK), containing a trapezoid Ge crystal (52 × 20 × 2 mm; Korth Kristalle, Altenholz, Germany) as an internal reflection element, was used in a Vertex 80V FTIR spectrometer (Bruker, Berlin, Germany). The internal mercury cadmium telluride detector was cooled with liquid nitrogen. A 45° incidence angle was used inside the Ge crystal, resulting in a total of 25 internal reflections, among which effectively 11 were utilized (sample flowthrough only on one side of the Ge surface). We mounted the Ge crystal with silicone sealings into the flowthrough cell. Liquid samples passed through the cell with a constant flow rate of 1 mL/min controlled by a peristaltic pump (Ismatec, Wertheim, Germany). The dead volume of the flow-cell amounted to 600 μL. All spectra were detected with an instrument resolution of 2 cm^{-1} and a factor 4 zero filling. Recorded reference spectrum and the sample spectrum were averaged over 1200 interferograms (mirror velocity 80 kHz), respectively, before the Fourier transformation. Using Fourier transformation, interferograms were converted into single-chain spectra, which were used to calculate the absorbance spectra according to Lambert-Beer's law. For each functionalization step, the aqueous solution was used as reference (here a 2-propanol, silanized surface or a buffer, antibody, or casein-coated saturated surface in equilibrium states). To ensure that EGCG did not have any structural effect on the functionalized sensor surface, we incubated the antibody-terminated and casein-saturated sensor surface with EGCG, analogously to the preparation protocols in the following sections.

Data correction

Spectral preprocessing was performed using built-in and in-house tools programmed with MATLAB 2016b (The MathWorks, Natick, MA). Spectral contributions of water vapor were eliminated by scaled subtraction using a reference spectrum. High-frequency noise was removed by a Fourier low-pass filter. For baseline correction, the absorbance was set to zero at five interpolation points (1000, 1485, 1750, 2700, and 3970 cm^{-1}). Spectral contributions of EGCG were eliminated by scaled subtraction using a pure EGCG absorbance spectrum. The absorbance band at 1148 cm^{-1} was used

Please cite this article in press as: Acharya et al., The Effect of (−)-Epigallocatechin-3-Gallate on the Amyloid-β Secondary Structure, Biophysical Journal (2020), https://doi.org/10.1016/j.bpj.2020.05.033

as a scaling factor because this band is not present in the absorbance spectra of monomeric or fibrillar Aβ. Please note that the spectra of EGCG with and without a functionalized surface are almost identical (Fig. S1). Therefore, no extra correction because of oxidation is required. To check the effect of counterions, we performed ATR-FTIR experiments with varying concentrations of counterions (Fig. S2). The counterion solutions were prepared in phosphate-buffered saline buffer. We concluded that the concentration of the counterions does not influence the secondary structure of $A\beta_{42}$.

Treatment of fibrillar Aβ with EGCG

Fibrillar $A\beta_{42}$ (36 nM; for fibril preparation, see above) was immobilized on the sensor surface for 60 min. Unbound Aβ was rinsed with phosphate-buffered saline buffer until equilibrium in the amide-II absorbance was observed. Aβ immobilization was performed with the monoclonal MOAB-2 antibody (Novus Biologicals, Wiesbaden-Nordenstadt, Germany), which is specific to the first four N-terminal amino acids of full-length Aβ. These fibrillar Aβ isoforms were treated with buffer containing 320 nM EGCG (Sigma-Aldrich) for at least 1 day in a circulating flow under red light. Infrared-difference absorbance spectra were continuously recorded.

Inhibition of Aβ aggregation with EGCG

Monomeric $A\beta_{42}$ (36 nM) was dissolved in buffer containing 320 nM EGCG and immediately immobilized on the functionalized sensor surface on monoclonal MOAB-2 antibody. The sample was passed over the flow-through cell in a circulating flow for at least 1 day to ensure identical incubation time on the sensor as fibrils. Afterwards, unbound monomeric Aβ was rinsed with phosphate buffer until equilibrium in the amide-II absorbance was observed. The difference absorbance spectra were continuously recorded.

Computational details

The structures of Aβ isoforms were obtained from the Protein Data Bank (PDB). For the monomeric form, we used the structure reported by Tomaselli et al. (36). For the fibrillar Aβ, we used four different PDB structures: 5OQV (37), 2BEG (38), 2NAO (39), and 2MXU (40). The monomer contains helix, turns, and coils in its secondary structure. On the contrary, the fibrillar Aβ consists of mainly extended configurations of β-sheets and β-turns.

Docking and MD simulation

We optimized the EGCG molecule at B3LYP/6-31+g(d,p) level of theory in a CPCM implicit water model 41). The optimized EGCG was then used for docking calculations on the $A\beta_{42}$ fibril. Docking calculations were performed using the Schrödinger suite (42). For MD simulation of the docked complex, we used the CHARMM36m force field (43) for the protein. The force-field parameters for the EGCG molecule were obtained from CGenFF (44), which assigns them by analogy to existing CHARMM parameters. Reliability of the CGenFF-generated parameters was indicated by the highest penalty for charge assignment of only 23. Before the final MD simulation, we minimized the Aβ + EGCG system and equilibrated the water box by freezing the Aβ and EGCG molecules. Subsequent equilibration of the entire system was performed first with a 2 kcal/mol/Å^2 restraint on the backbone atoms for 1 ns, followed by a 10-ns equilibration without restraints. This equilibration procedure was performed using NAMD (45) with a 2-fs time step. Production MD simulation was performed using Amber (46) at a constant temperature of 310 K and a constant pressure of 1 atm in a TIP3P (47) water box. The particle mesh Ewald method (48) was used to compute electrostatic interactions in alternate time steps. A 12-Å cutoff with a switching function from 10 to 12 Å was used in our simulation. Analysis of the simulation was performed with VMD (49). Snapshots were collected every 200 ps for further analysis.

Divide-and-conquer approach

The model monomer structure was analyzed to investigate structures with predominantly helical and coil components. Model dimers were analyzed to investigate interchain hydrogen bonding between β-sheets (Fig. 1 *C*). In each case, the starting model was divided into several smaller fragments. Sample fragmentation schemes are shown in Fig. 1, *A* and *B*. To mimic the native secondary structure, each fragment was partially optimized while freezing the backbone dihedral angles (as in (34)) at the BP86/TVZP level of theory, followed by a frequency calculation at the same level of theory. Additionally, in the case of a dimer model, distances between the α-carbon atoms of the same residues from each chain were frozen during the optimization procedure. Each calculation was performed in the CPCM implicit water model (41). The frequencies of the normal modes from each fragment were then collected in the range 1400–1900 cm^{-1}, followed by convolution of the spectrum using a Gaussian of width 5 cm^{-1}. The convoluted spectrum of each fragment was then added to obtain the final spectra. All electronic structure calculations were performed using the Gaussian16 software package (50).

RESULTS AND DISCUSSION

Measurements with the immuno-infrared sensor

We used the immuno-infrared sensor to characterize the effect of EGCG on the formation and remodeling of $A\beta_{42}$ peptides. Therefore, we analyzed the difference in the absorption spectra of $A\beta_{42}$ peptides in the presence and absence of EGCG over time. $A\beta_{42}$ spectra are obtained by immobilizing $A\beta_{42}$ on a surface functionalized with monoclonal antibody MOAB-2. One surface was incubated with monomeric $A\beta_{42}$, and the other one with fibrillar $A\beta_{42}$. The antibody MOAB-2 is specific to the N-terminus of $A\beta_{42}$ (residues 1–4) and thus recognizes both monomeric and fibrillar $A\beta_{42}$ isoforms. Both isoforms are likely to exhibit several conformations consistent with structures deposited in the PDB for Aβ. Our measurement after 0 min of monomeric $A\beta_{42}$ peptide (Fig. 2, *red spectrum*) shows an amide-I absorbance maximum at 1654 cm^{-1}, which corresponds to dominant helical and coil content (31,51), indicating that nonfibrillar $A\beta_{42}$ is bound to the sensor surface. The bound nonfibrillar $A\beta_{42}$ are most likely monomers. However, we cannot definitively exclude spherical or other types of aggregates with high helical and coil content. In contrast, the absorption spectrum of fibrillar $A\beta_{42}$ (Fig. 2, *blue spectrum*) exhibits a significantly shifted amide-I band with a maximum at 1628 cm^{-1}, corresponding to a high content of β-sheet structures (31,51), indicating that $A\beta_{42}$ fibrils are bound to the sensor surface.

To measure the changes in the secondary structure of fibrillar $A\beta_{42}$ upon EGCG treatment, 36 nM of freshly prepared fibrillar $A\beta_{42}$ peptide (see Experimental Details) was immobilized on the sensor surface and treated with 320 nM EGCG in a circulating flow. We found that the amide-I frequency maximum shifted from 1628 to 1638 cm^{-1} after 1 day (Fig. 3 *A*), and the amide-I band became broader between 1640 and 1660 cm^{-1} after the addition of EGCG. These observations point toward increased helix and

Please cite this article in press as: Acharya et al., The Effect of (−)-Epigallocatechin-3-Gallate on the Amyloid-β Secondary Structure, Biophysical Journal (2020), https://doi.org/10.1016/j.bpj.2020.05.033

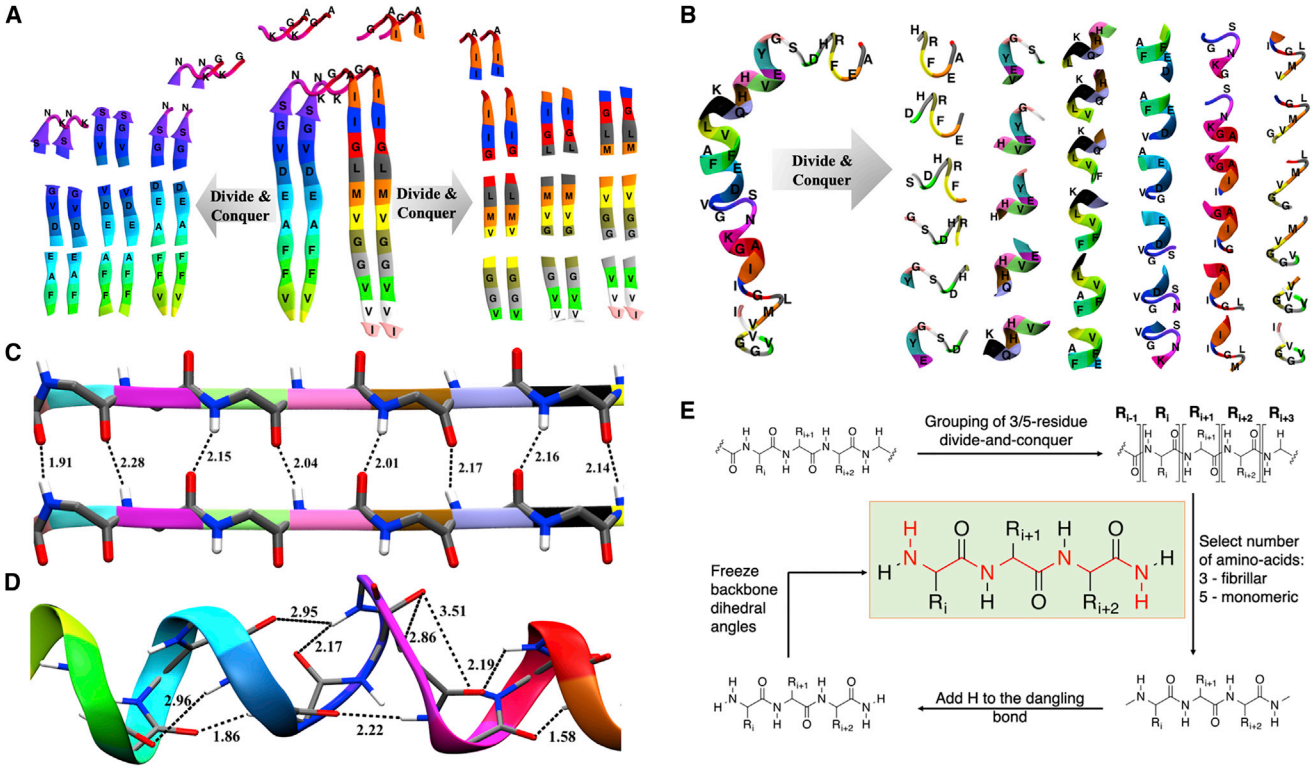

FIGURE 1 Illustration of fragmentation procedure for model (*A*) dimeric and (*B*) monomeric Aβ. Each fragment contains five amino acids and thus includes all possible intrachain H-bonding observed in a helical structure. The hydrogen-bonding network in (*C*) monomeric and (*D*) dimeric fibril (*bottom*) models is shown. Individual amino acids are shown in different colors. (*E*) Illustration of the setup for the divide-and-conquer approach and representation of an individual fragment subjected to partial optimization and the subsequent frequency calculation are shown. To see this figure in color, go online.

random-coil content in $A\beta_{42}$ in the presence of EGCG. We interpret this change in shape (and maxima) of the absorption spectra as conformational changes of the $A\beta_{42}$ fibril into nonamyloid aggregates without disassembly. Treatment of fibrillar $A\beta_{42}$ with EGCG for longer times such as 1 day (Fig. 3 *A*, *red spectra*) did not significantly affect the spectra beyond the changes induced by the 90-min treatment (Fig. 3 *A*, *green spectra*).

Remarkably, preincubation of 36 nM monomeric $A\beta_{42}$ with 320 nM EGCG prevented fibril formation for 1 day (Fig. 3 *B*). We dissolved $A\beta_{42}$ monomer in a buffered solution of 320 nM EGCG and directly immobilized it on the sensor surface. The immobilized fraction was further incubated with 320 nM EGCG in a circulating flow. After 1 day of EGCG treatment, the amide-I maximum remained stable around 1647 cm^{-1}, suggesting that the immobilized $A\beta_{42}$ has a high content of disordered or coil or helical secondary structure elements under these conditions (buffer + EGCG). We note that we could not completely inhibit fibril or oligomer formation. Therefore, a tiny fraction of them may still be present in this sample, which is consistent with results previously demonstrated by other research groups (23,24). Thus, the spectra of the monomer are broader than usual. Nevertheless, the dominant fraction of the immobilized Aβ was coil or helical in nature. Further aggregation into the β-sheet enriched structure was prevented by EGCG.

As a control, we prepared monomeric $A\beta_{42}$ in a buffer solution without EGCG before immobilization on a freshly functionalized sensor surface. The immobilized $A\beta_{42}$ fraction and the circulating $A\beta_{42}$ peptides rapidly aggregated, forming β-sheet enriched species within the first 60 min, eventually leading to the formation of mature Aβ fibrils within a day (Fig. 3 *C*), as seen from the shift in the amide-I maxima from 1654 cm^{-1} → 1641 cm^{-1} → 1632 cm^{-1} → 1628 cm^{-1}. It is noteworthy that the maximum of 1654 cm^{-1} at 20 min and the final maximum of 1628 cm^{-1} after 1 day were also observed in the amide-I maxima of the monomer and fibril, respectively (Fig. 2). Additionally, we incubated a freshly functionalized sensor surface with EGCG in the absence of Aβ, finding that EGCG did not alter the functionalized sensor surface and that the observations with EGCG and Aβ experiments exclusively reflect structural changes of Aβ (Fig. S3).

EGCG binding and hydrogen-bonding interactions

Identifying specific interactions between Aβ and EGCG are critical for understanding the perturbative effects of EGCG

Please cite this article in press as: Acharya et al., The Effect of (−)-Epigallocatechin-3-Gallate on the Amyloid-β Secondary Structure, Biophysical Journal (2020), https://doi.org/10.1016/j.bpj.2020.05.033

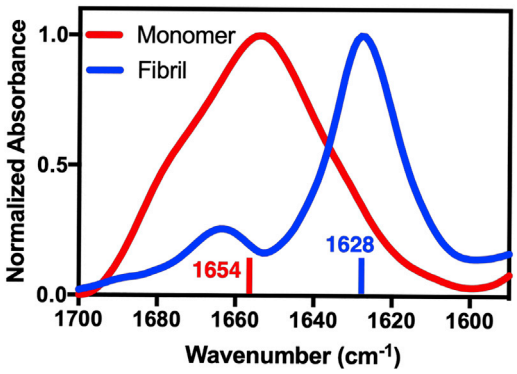

FIGURE 2 Experimental IR spectra of monomeric (*red*) and fibrillar $A\beta_{42}$ (*blue*) measured directly after 0 min. The peak of the absorption band of fibrillar $A\beta_{42}$ at 1628 cm^{-1} corresponds to the amide-I stretching vibrational mode of β-sheets, which is at 1630 cm^{-1} (31,51), indicating that $A\beta_{42}$ fibrils are actually immobilized on the sensor surface. The peak of monomeric $A\beta_{42}$ at 1654 cm^{-1} corresponds to the amide-I stretching vibrational mode of helical or coil secondary structure, indicating a nonfibrillar structure. To see this figure in color, go online.

on Aβ. Therefore, we performed docking calculations to locate interaction sites around and inside the Aβ fibril using GLIDE (52). We selected a recent cryo-electron microscopy structure (37) of $A\beta_{42}$ as the receptor because it contains the full amino acid sequence, i.e., residues 1–42. Docking calculations revealed three binding sites of EGCG, shown in Fig. 4 *A*, that were ranked according to the GlideScore. We found that the most favorable GlideScore (−6.9; docking site #1) was obtained when EGCG binds inside the fibril, stabilized by π-stacking interactions with amino acid residue Phe19. A similar folding pattern is also observed in $A\beta_{40}$ around the Phe19 residue, which participates in a "steric-zipper" interaction with another hydrophobic residue (53). Mutations of Phe19 lead to reduced toxicity of $A\beta_{40}$ (54). One can expect similar effects in $A\beta_{42}$. Indeed, $A\beta_{42}$-F19S and $A\beta_{42}$-F19D mutants are less prone to aggregate than the wild-type $A\beta_{42}$ (55,56). In addition, EGCG is further stabilized in site #1 by interactions with the backbone of Ile31, Ala30, Gly29, Lys28, and Asn27 residues of $A\beta_{42}$ (Fig. 4 *B*). These results are also consistent with earlier studies, which suggested that EGCG interacts directly with Aβ (29). These interactions may weaken the interchain and steric-zipper-type interactions (53), which have been implicated in the fibrillation process (57–59).

The next two docking sites are comparable, despite the differences in the type of interactions with $A\beta_{42}$. The second docking site is near the N-terminus of $A\beta_{42}$. EGCG is stabilized by hydrophilic interactions in this docking site because the N-terminus is dominated by acidic or basic amino acid residues. Conversely, the third docking site is in the C-terminal region of $A\beta_{42}$, where EGCG is stabilized by hydrophobic interaction with the Ile41 and Ala42 side chain and hydrophilic interactions with the C-terminus and the side chain of Lys 28 (see Fig. S5). Mutations of these terminal hydrophobic residues are shown to reduce $A\beta_{42}$ aggregation (55). Additionally, EGCG interrupts the salt bridge between the C-terminus and Lys28, which is crucial for the stability of the S-shaped Aβ fibril (60). Conversely, this salt bridge is replaced by Asp23 and Lys28 in $A\beta_{40}$, which is important for $A\beta_{40}$ oligomer formation (61,62). Furthermore, a pivotal hydrophobic contact between Phe19 and Leu34 in $A\beta_{40}$ (54,63) is possibly replaced by a Phe19-Ile31 hydrophobic contact in $A\beta_{42}$ (see Fig. 4 *A*). Mutations of either of these residues lead to reduced aggregation tendency of the $A\beta_{42}$

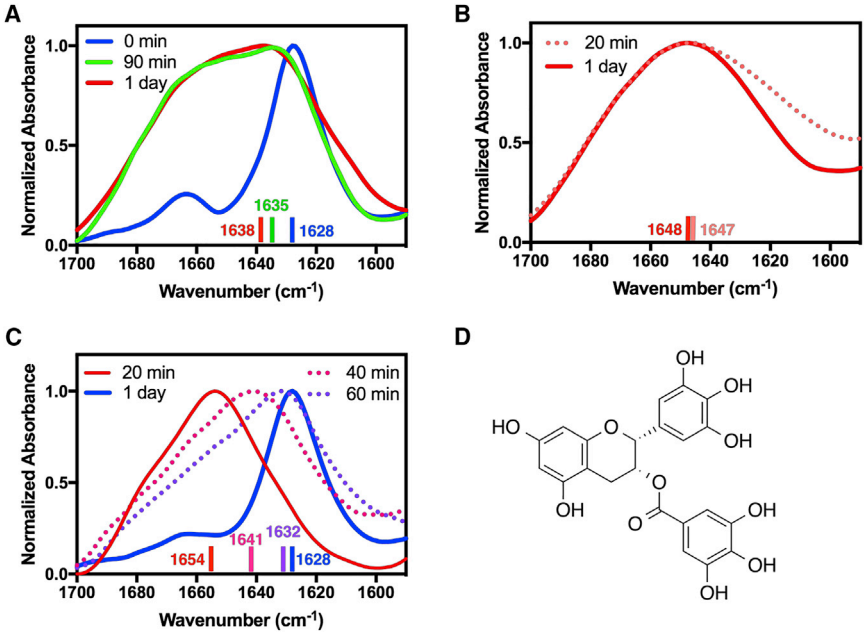

FIGURE 3 (*A*) Spectra of fibrillar $A\beta_{42}$ after immobilization on the immuno-infrared sensor and treatment with EGCG for 1 day. (*B*) Spectra of preincubated monomeric Aβ with EGCG, which prevents the formation of fibrillar species, are shown. The concentrations of Aβ fibril, monomer, and EGCG in (*A*) and (*B*) were 36, 36, and 320 nM, respectively. (*C*) Spectra corresponding to the evolution of $A\beta_{42}$ fibrils from monomers in the absence of EGCG are shown. (*D*) The chemical structure of EGCG is shown. To see this figure in color, go online.

Please cite this article in press as: Acharya et al., The Effect of (−)-Epigallocatechin-3-Gallate on the Amyloid-β Secondary Structure, Biophysical Journal (2020), https://doi.org/10.1016/j.bpj.2020.05.033

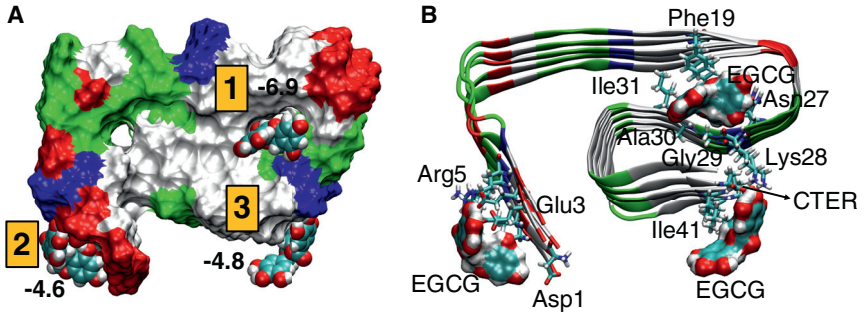

FIGURE 4 (*A*) EGCG binding sites (numbered 1–3) in Aβ_{42} with respective docking scores. Aβ_{42} is shown in surface representation and colored by residue type: hydrophobic (*white*), acidic (*red*), basic (*blue*), and polar (*green*). EGCG molecules in each site are shown in van der Waals representation. (*B*) Interacting residues of Aβ_{42} with EGCG in each docking pose are shown. To see this figure in color, go online.

(55,56). Curcumin is shown to disrupt salt bridges around the C-terminus, leading to disruption of Aβ aggregates (20,64). Because of similarities in the structural elements (polyphenolic and aromatic) between curcumin and EGCG, the C-terminal EGCG interaction site should also disrupt the salt bridges present in Aβ_{42}, leading to the destruction of Aβ_{42} aggregates.

We analyzed stability of EGCG in the three docking sites by performing MD simulations over an extended 1-μs trajectory. The average Aβ_{42}-EGCG distances over the whole simulation time were 2.67, 2.70, and 1.78 Å. Therefore, we concluded that EGCG is stable in the identified docking sites even in the presence of thermal nuclear fluctuations and remains in close contact with the Aβ_{42} fibril throughout the entire duration of the simulation. An additional docking site (*site #4* in Fig. 5) was also identified by the MD simulations, where EGCG is stabilized by both hydrophilic and hydrophobic interactions. Site #4 is populated by multiple EGCG molecules during a significant fraction of the simulation. To analyze the occupancy of a docking site, we identified interacting residues that define it, followed by computation of the distance between an EGCG molecule and the residue(s). When the computed distance is less than 5 Å, we identify the site as occupied followed by a count of EGCG molecules in it. Because the size of the EGCG molecule is fairly large, it can interact with multiple docking sites at once depending on the pose. The residues defining each site are the following: site #1, Phe19; site #2, Glu3; site #3, Ile41; and site #4, Glu11 and His13. The relative population of each docking site is shown in Fig. 5 *D*. Because there are only three EGCG molecules present in the system, the maximal possible population is three. We observe that although the populations of sites #1–3 are comparable to one another, site #4 is distinctly more populated. The multiple occupancies of EGCG also occur most frequently in site #4 compared with any other site. Conversely, smaller molecules like scyllo-inositol and homotaurine interact with Aβ in a nonspecific manner (65). Small peptides may bind to amyloid in a specific manner without leading to the disruption of the oligomeric or fibrillar structure, as recently demonstrated by Levine et al. for hiAPP using mitochondrially derived peptides (66). Therefore, EGCG-based molecules can be better suited for optimization of interactions between Aβ

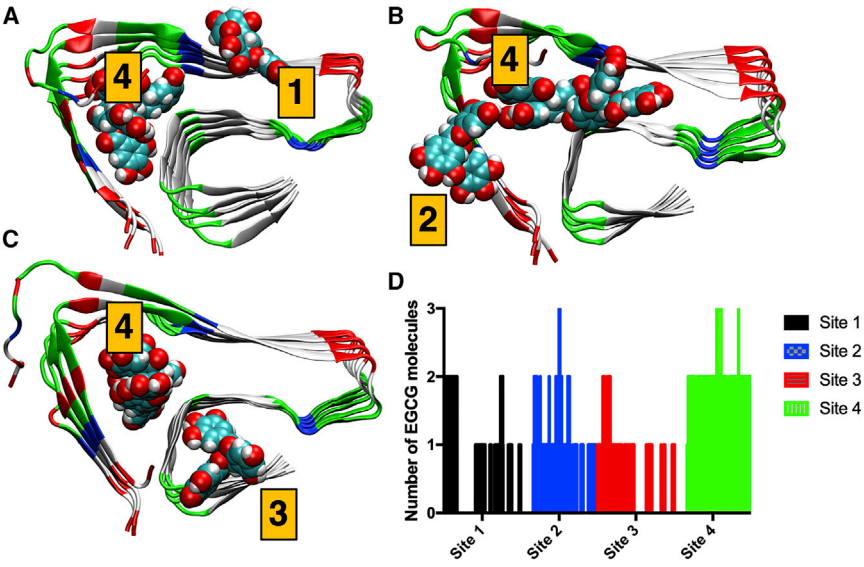

FIGURE 5 Representative figures of EGCG occupying (*A*) site #1 and site #4, (*B*) site #2 and site #4, and (*C*) site #3 and site #4. (*D*) The relative populations of the docking sites from MD simulation are shown. The populations are grouped by their site numbers. Aβ42 is colored by residue type: hydrophobic (*white*), acidic (*red*), basic (*blue*), and polar (*green*). EGCG molecules are shown in van der Waals representation. To see this figure in color, go online.

Please cite this article in press as: Acharya et al., The Effect of (−)-Epigallocatechin-3-Gallate on the Amyloid-β Secondary Structure, Biophysical Journal (2020), https://doi.org/10.1016/j.bpj.2020.05.033

and small molecules, leading to disruption of oligomeric and fibrillar Aβ. Mixed hydrophilic and hydrophobic interactions between Aβ were initially proposed by Sun and coworkers (67,68). Their study also showed that the binding free energy increases in the order Aβ1–30 > Aβ31–42 > Aβ1–16 (68). Therefore, interaction sites #1 and/or #4 should be favored more energetically. However, switching between these sites is highly likely, as observed in our simulations, because the difference in free energy between them is on the order of 1 kcal/mol (68).

It is also reported that the initial binding of EGCG, which leads to preferential intramolecular interactions in Aβ, may facilitate recruitment of more EGCG molecules (69). Lastly, Hyung et al. highlighted the importance of His6, His13, and His14 in EGCG-$A\beta_{40}$ interactions (69). We observed similar interactions at site #4 of the EGCG-$A\beta_{42}$ system.

Although complete disruption of the $A\beta_{42}$ fibril cannot be captured in the timescale of the MD simulation, we are able to rationalize the difference between the amide-I maxima (Fig. 2) and the observed shift in the presence and the absence of EGCG (Fig. 3) using the $A\beta_{42}$ monomer and fibril structures. To account for the structural variation in the Aβ fibrils, we used four different fibril models (Fig. 6, *A–D*) with distinct shapes and β-sheet contents. We quantified the secondary structure of each model by using the Timeline plugin of VMD (49), summarized in Table 1. We used the default definitions of secondary structure components as encoded in the VMD (49). It is noteworthy that among the four selected $A\beta_{42}$ fibril structures, only two (PDB: 5OQV and 2NAO) contain the full sequence of $A\beta_{42}$. PDB: 2MXU and 2BEG contain residues 11–42 and 17–42, respectively. The β-sheet content of 5OQV, 2MXU, and 2BEG is comparable (71–77%), whereas it is quite low for 2NAO (31%). 2NAO has similar β-sheet (31%), turn (36%), and coil (33%) content, with the last being the highest among all model fibrils. Nevertheless, all the fibril models have strong interchain hydrogen bonds. Surprisingly, only 2NAO has a partial disruption of the interchain hydrogen bonds between residues 9 and 12. Fig. 6 *E* illustrates the broken interchain hydrogen-bonding network characterized by much longer interchain distances compared with the rest of the structures.

We computed the IR spectra of models of $A\beta_{42}$ fibril and one monomer (PDB: 1ZOQ). Fig. 7 and Table 1 summarize the amide-I maxima obtained using each of the model structures. The amide-I shift for fibrillar → monomeric transition or vice versa is estimated as the difference between the amide-I maxima obtained from the fibrillar PDB structures and the PDB: 1ZOQ structure. We found that positions of the maxima are very similar for all the fibril models, ranging from 1612 to 1621 cm^{-1}, which are very close to the experimental fibrillar maximum of 1628 cm^{-1}. Additionally, the computed maximum (1645 cm^{-1}) for the monomeric model is very close to the experimental monomeric maximum (1654 cm^{-1}). More importantly, the computed frequency shift for the models (24–33 cm^{-1}) matches the experimental shift of 26 cm^{-1}, with full-length $A\beta_{42}$ models (24–29 cm^{-1}) being closer to the experiments than $A\beta_{11-42}$ and $A\beta_{17-42}$ (31–33 cm^{-1}).

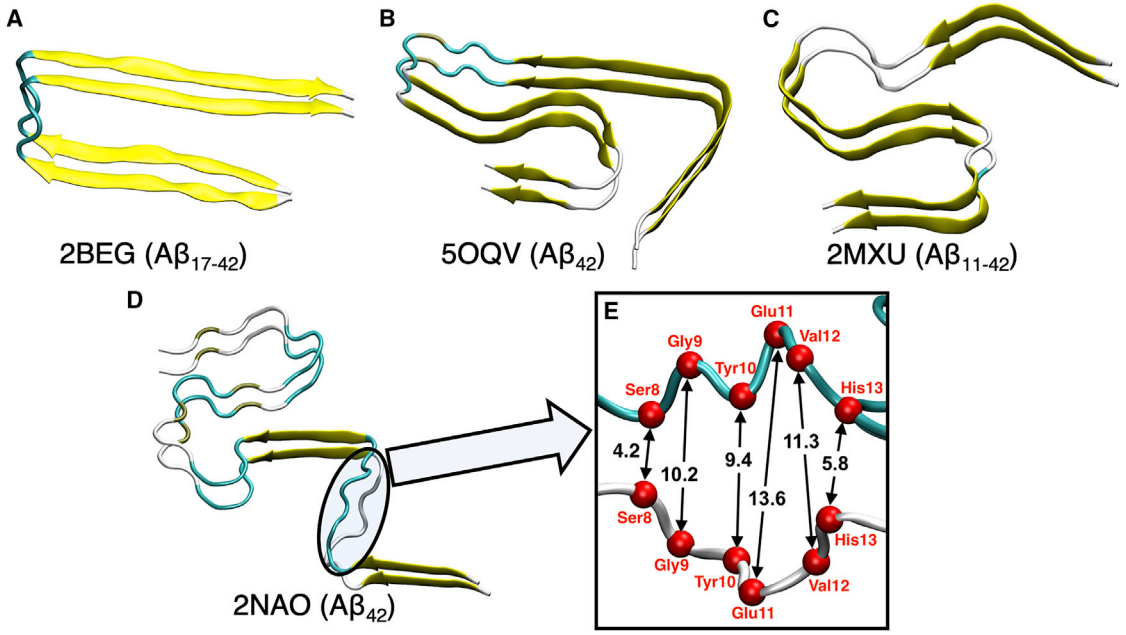

FIGURE 6 Dimer models of fibrillar A used in the divide-and-conquer approach from four different PDB entries: (*A*) 2BEG, (*B*) 5OQV, (*C*) 2MXU, and (*D*) 2NAO. (*E*) Partial disruption of interchain hydrogen bonding observed for one of the structures used for computation is shown. The relevant residues are annotated in red, and the α-carbons of those residues are shown as red spheres. To see this figure in color, go online.

Please cite this article in press as: Acharya et al., The Effect of (−)-Epigallocatechin-3-Gallate on the Amyloid-β Secondary Structure, Biophysical Journal (2020), https://doi.org/10.1016/j.bpj.2020.05.033

TABLE 1 Comparison of Computational and Experimental IR Frequencies and Frequency Shifts for Aβ Isoforms

	Secondary structure (PDB−system)	β[a] %	Turn %	Helix[b] %	Coil %	amide-I maxima (cm^{-1})	Frequency shift (cm^{-1})
Computational	Monomeric (1ZOQ)	0	50	43	7	1645	
	Fibrillar (5OQV)	71	12	0	17	1616	29
	Fibrillar (2NAO)	31	36	0	33	1621	24
	Fibrillar (2MXU)	72	2	0	27	1614	31
	Fibrillar (2BEG)	77	15	0	8	1612	33
Experimental	Monomeric	-				1654	
	Fibrillar	-				1628	26

[a] β content = extended configuration content + isolated bridge content
[b] Helix content = α-helix content + 3-10 helix content + π-helix content.

The secondary structures were calculated as defined in the Timeline plugin of the VMD package (49).

Interestingly, the intensities of the maxima in the region between 1640 and 1660 cm^{-1} directly correlate with the coil content of the systems (Fig. 7 *A*; Table 1), i.e., the intensity of this peak increases with higher coil content. For example, coil content in the PDB structures, and hence the intensity of the band between 1640 and 1660 cm^{-1}, increases in the order 2NAO < 2MXU < 5OQV < 2BEG. The intensity of the peak decreases when we remove the contributions from residues 9 to 12 from IR calculations of the 2NAO structure (Fig. 7 *B*). Therefore, broken interchain hydrogen bonds also contribute to the band in this region (Fig. 6 *E*).

We anticipate that the binding of EGCG molecules in the space between Phe19 and Ala30 (site #1) might produce an effect similar to the formation of a disulfide bridge in an A21C-A30C mutant (70). These mutations induce a hairpin structure that stabilizes the monomeric form of Aβ (patent, WO 2009/128772 A1)). In contrast, cysteine mutations of other residues such as Ala2, Ser8, Ser26, and Ala42 do not affect fibril formation. Nevertheless, EGCG docked into all the binding sites may interfere with the interchain interactions suggesting that EGCG-Aβ interactions block the interchain hydrogen bonds. Therefore, one can expect to observe stronger C=O bonds in the monomeric Aβ in the β-sheet-enriched structure. We confirmed that hypothesis by computing the IR spectra of a model β-enriched monomer using only one chain from the 5OQV fibril structure, a model monomer completely devoid of interchain hydrogen bonds. As anticipated, we observed that the monomer amide-I maximum is shifted 13 cm^{-1} relative to the model dimer, as shown in Fig. 8. The interactions between protofilaments are also important for the structural integrity of fibrils. Usually, protofilament interactions protect the C-terminal hydrophobic stretch from solvent exposure. Herein, we note that the C-terminus of one protofilament is close to the N-terminus of another protofilament (37). Therefore, interaction sites #2 and #3 will collapse to a single site in a mature fibril, possibly with multiple occupancy. Sites #1 and #4 may be inaccessible to solvent initially. However, the hydrophobic nature of EGCG-Aβ_{42} interactions at these sites should make it more accessible to EGCG. Regardless, a prior report shows that initial binding of EGCG induces binding of more EGCG molecules, possibly in other sites (69). Large-scale simulation with periodic unit of protofibrils may shed light onto the details of such interactions.

CONCLUSION

We have analyzed the effect of EGCG binding on the secondary structure of Aβ_{42} combining in vitro immuno-infrared measurements, MD simulation, and ab initio

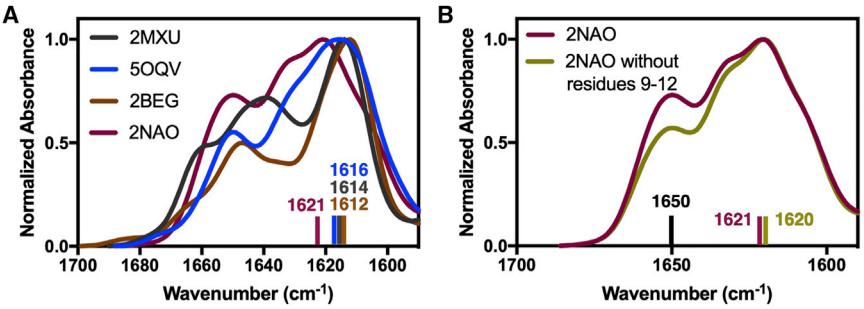

FIGURE 7 Analysis of the computed IR spectra in the 1600–1700 cm^{-1} region. (*A*) Comparison of IR spectra of all the fibril models is shown. (*B*) A comparison of IR spectra of 2NAO structure with and without the broken interchain hydrogen-bonding residues is shown. To see this figure in color, go online.

Please cite this article in press as: Acharya et al., The Effect of (−)-Epigallocatechin-3-Gallate on the Amyloid-β Secondary Structure, Biophysical Journal (2020), https://doi.org/10.1016/j.bpj.2020.05.033

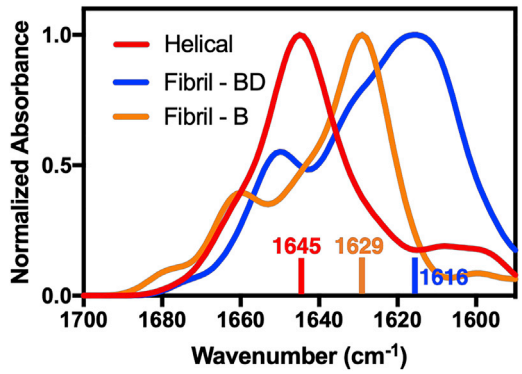

FIGURE 8 Comparison of the computed amide-I band in monomeric (*orange*) and dimeric $A\beta_{42}$ (*blue*) in β-enriched structures. IR spectrum of monomeric $A\beta_{42}$ (*red*) is also shown for reference. To see this figure in color, go online.

calculations of the amide-I maxima for monomeric and fibrillar $A\beta_{42}$ model structures. The analysis of EGCG binding revealed favorable interactions with the β-sheet-enriched Aβ. The interaction sites stabilize EGCG through hydrophilic interactions with the Aβ backbone, as well as specific side-chain interactions with key amino acid residues and π-stacking interactions with aromatic amino acids. An extended long (1-μs) MD simulation revealed an additional interaction site of EGCG, which is more populated than others identified by docking calculations. We also found that docking sites with multiple EGCG molecules were significantly populated. Moreover, EGCG disrupts the interchain hydrogen bonds and salt bridges, which are crucial for the fibril structure and shape of Aβ.

This study serves as a proof of principle for combining computational analysis and IR spectra calculations with experimental data analysis using an immuno-infrared sensor to study interactions between Aβ and small molecules. The interaction sites identified in this work provide a starting point for follow-up experimental investigations of drug-Aβ interactions in greater detail. Moreover, the combined strategy may further contribute to rational drug designs by unraveling the molecular interactions that lead to the disruption of β-sheet-enriched Aβ by small drug-like molecular inhibitors.

SUPPORTING MATERIAL

Supporting Material can be found online at https://doi.org/10.1016/j.bpj.2020.05.033.

AUTHOR CONTRIBUTIONS

A.A., A.N., K.G., and V.S.B. designed the research. A.A. and J.C.G. carried out all calculations and analyzed the data. J.S., L.B., and A.N. performed the experiments and analyzed the data. A.A., J.S., L.B., T.R., A.N., J.C.G., and V.S.B. wrote the manuscript.

ACKNOWLEDGMENTS

The authors thank Dr. Benjamin Rudshteyn for his help with writing the dihedral freezing code.

Financial support was provided by the National Institutes of Health grants 2R01GM106121-01A1 (V.S.B.), the Ministry of Culture and Science of North Rhine-Westphalia through grant 111.08.03.05-133974 (K.G.), the Protein Research Unit Ruhr within Europe funded by the Ministry of Innovation, Science and Research of North Rhine-Westphalia (K.G.), and R01-GM123169 (J.C.G.). Supercomputer time was provided by NERSC and the Yale University Faculty of Arts and Sciences High Performance Computing Center partially funded by the National Science Foundation grant CNS 08-21132. Supercomputing time was also provided by the Extreme Science and Engineering Discovery Environment under grant numbers TG-CHE170024 and TG-MCB130173 and the Partnership for an Advanced Computing Environment at the Georgia Institute of Technology, Atlanta, Georgia.

REFERENCES

1. Alzheimer's Association. 2018. 2018 Alzheimer's disease facts and figures. *Alzheimers Dement.* 14:367–429.
2. Hardy, J., and D. J. Selkoe. 2002. The amyloid hypothesis of Alzheimer's disease: progress and problems on the road to therapeutics. *Science.* 297:353–356.
3. Dohler, F., D. Sepulveda-Falla, …, M. Glatzel. 2014. High molecular mass assemblies of amyloid-β oligomers bind prion protein in patients with Alzheimer's disease. *Brain.* 137:873–886.
4. Teplow, D. B., N. D. Lazo, …, H. E. Stanley. 2006. Elucidating amyloid β-protein folding and assembly: a multidisciplinary approach. *Acc. Chem. Res.* 39:635–645.
5. Mousseau, N., and P. Derreumaux. 2005. Exploring the early steps of amyloid peptide aggregation by computers. *Acc. Chem. Res.* 38:885–891.
6. Tycko, R., and R. B. Wickner. 2013. Molecular structures of amyloid and prion fibrils: consensus versus controversy. *Acc. Chem. Res.* 46:1487–1496.
7. Ban, T., K. Yamaguchi, and Y. Goto. 2006. Direct observation of amyloid fibril growth, propagation, and adaptation. *Acc. Chem. Res.* 39:663–670.
8. Hamley, I. W. 2012. The amyloid beta peptide: a chemist's perspective. Role in Alzheimer's and fibrillization. *Chem. Rev.* 112:5147–5192.
9. Klein, W. L., W. B. Stine, Jr., and D. B. Teplow. 2004. Small assemblies of unmodified amyloid β-protein are the proximate neurotoxin in Alzheimer's disease. *Neurobiol. Aging.* 25:569–580.
10. Matsuzaki, K. 2014. How do membranes initiate Alzheimer's Disease? Formation of toxic amyloid fibrils by the amyloid β-protein on ganglioside clusters. *Acc. Chem. Res.* 47:2397–2404.
11. Kreutzer, A. G., and J. S. Nowick. 2018. Elucidating the structures of amyloid oligomers with macrocyclic β-hairpin peptides: insights into Alzheimer's disease and other amyloid diseases. *Acc. Chem. Res.* 51:706–718.
12. Bate, C., S. Kempster, …, A. Williams. 2006. Interferon-γ increases neuronal death in response to amyloid-β1-42. *J. Neuroinflammation.* 3:7.
13. Milanesi, L., T. Sheynis, …, H. R. Saibil. 2012. Direct three-dimensional visualization of membrane disruption by amyloid fibrils. *Proc. Natl. Acad. Sci. USA.* 109:20455–20460.
14. Bamberger, M. E., M. E. Harris, …, G. E. Landreth. 2003. A cell surface receptor complex for fibrillar β-amyloid mediates microglial activation. *J. Neurosci.* 23:2665–2674.
15. Butterfield, D. A., J. Drake, …, A. Castegna. 2001. Evidence of oxidative damage in Alzheimer's disease brain: central role for amyloid β-peptide. *Trends Mol. Med.* 7:548–554.

16. Bemporad, F., G. Calloni, …, F. Chiti. 2006. Sequence and structural determinants of amyloid fibril formation. *Acc. Chem. Res.* 39:620–627.

17. vandenAkker, C. C., M. F. M. Engel, …, G. H. Koenderink. 2011. Morphology and persistence length of amyloid fibrils are correlated to peptide molecular structure. *J. Am. Chem. Soc.* 133:18030–18033.

18. Rezai-Zadeh, K., D. Shytle, …, J. Tan. 2005. Green tea epigallocatechin-3-gallate (EGCG) modulates amyloid precursor protein cleavage and reduces cerebral amyloidosis in Alzheimer transgenic mice. *J. Neurosci.* 25:8807–8814.

19. Marambaud, P., H. Zhao, and P. Davies. 2005. Resveratrol promotes clearance of Alzheimer's disease amyloid-β peptides. *J. Biol. Chem.* 280:37377–37382.

20. Yang, F., G. P. Lim, …, G. M. Cole. 2005. Curcumin inhibits formation of amyloid beta oligomers and fibrils, binds plaques, and reduces amyloid in vivo. *J. Biol. Chem.* 280:5892–5901.

21. Frydman-Marom, A., A. Levin, …, M. Ovadia. 2011. Orally administrated cinnamon extract reduces β-amyloid oligomerization and corrects cognitive impairment in Alzheimer's disease animal models. *PLoS One.* 6:e16564.

22. Mishra, R., D. Sellin, …, R. Winter. 2009. Inhibiting islet amyloid polypeptide fibril formation by the red wine compound resveratrol. *ChemBioChem.* 10:445–449.

23. Ehrnhoefer, D. E., J. Bieschke, …, E. E. Wanker. 2008. EGCG redirects amyloidogenic polypeptides into unstructured, off-pathway oligomers. *Nat. Struct. Mol. Biol.* 15:558–566.

24. Bieschke, J., J. Russ, …, E. E. Wanker. 2010. EGCG remodels mature α-synuclein and amyloid-β fibrils and reduces cellular toxicity. *Proc. Natl. Acad. Sci. USA.* 107:7710–7715.

25. de Almeida, N. E. C., T. D. Do, …, M. T. Bowers. 2017. 1,2,3,4,6-penta-O-galloyl-β-D-glucopyranose binds to the N-terminal metal binding region to inhibit amyloid *β*-protein oligomer and fibril formation. *Int. J. Mass Spectrom.* 420:24–34.

26. Attanasio, F., M. Convertino, …, E. Rizzarelli. 2013. Carnosine inhibits Aβ(42) aggregation by perturbing the H-bond network in and around the central hydrophobic cluster. *ChemBioChem.* 14:583–592.

27. Arai, T., T. Araya, …, M. Kanai. 2014. Rational design and identification of a non-peptidic aggregation inhibitor of amyloid-β based on a pharmacophore motif obtained from cyclo[-Lys-Leu-Val-Phe-Phe-]. *Angew. Chem. Int.Ed.* 53:8236–8239.

28. Nasica-Labouze, J., P. H. Nguyen, …, P. Derreumaux. 2015. Amyloid β protein and Alzheimer's disease: when computer simulations complement experimental studies. *Chem. Rev.* 115:3518–3563.

29. Liu, F. F., X. Y. Dong, …, Y. Sun. 2011. Molecular insight into conformational transition of amyloid β-peptide 42 inhibited by (-)-epigallocatechin-3-gallate probed by molecular simulations. *J. Phys. Chem. B.* 115:11879–11887.

30. Schartner, J., A. Nabers, …, K. Gerwert. 2017. An ATR-FTIR sensor unraveling the drug intervention of methylene blue, congo red, and berberine on human Tau and Aβ. *ACS Med. Chem. Lett.* 8:710–714.

31. Nabers, A., J. Ollesch, …, K. Gerwert. 2016. An infrared sensor analysing label-free the secondary structure of the Aβ peptide in presence of complex fluids. *J. Biophotonics.* 9:224–234.

32. Nabers, A., J. Ollesch, …, J. Wiltfang. 2016. Amyloid-β-secondary structure distribution in cerebrospinal fluid and blood measured by an immuno-infrared-sensor: a biomarker candidate for Alzheimer's disease. *Anal. Chem.* 88:2755–2762.

33. Nabers, A., L. Perna, …, H. Brenner. 2018. Amyloid blood biomarker detects Alzheimer's disease. *EMBO Mol. Med.* 10:e8763.

34. Xiao, D., L. Fu, …, E. C. Y. Yan. 2012. Amphiphilic adsorption of human islet amyloid polypeptide aggregates to lipid/aqueous interfaces. *J. Mol. Biol.* 421:537–547.

35. Poojari, C., D. Xiao, …, B. Strodel. 2013. Membrane permeation induced by aggregates of human islet amyloid polypeptides. *Biophys. J.* 105:2323–2332.

36. Tomaselli, S., V. Esposito, …, D. Picone. 2006. The α-to-β conformational transition of Alzheimer's Aβ-(1-42) peptide in aqueous media is reversible: a step by step conformational analysis suggests the location of β conformation seeding. *Chembiochem.* 7:257–267.

37. Gremer, L., D. Schölzel, …, G. F. Schröder. 2017. Fibril structure of amyloid-β(1-42) by cryo-electron microscopy. *Science.* 358:116–119.

38. Lührs, T., C. Ritter, …, R. Riek. 2005. 3D structure of Alzheimer's amyloid-β(1-42) fibrils. *Proc. Natl. Acad. Sci. USA.* 102:17342–17347.

39. Wälti, M. A., F. Ravotti, …, R. Riek. 2016. Atomic-resolution structure of a disease-relevant Aβ(1-42) amyloid fibril. *Proc. Natl. Acad. Sci. USA.* 113:E4976–E4984.

40. Xiao, Y., B. Ma, …, Y. Ishii. 2015. Aβ(1-42) fibril structure illuminates self-recognition and replication of amyloid in Alzheimer's disease. *Nat. Struct. Mol. Biol.* 22:499–505.

41. Cossi, M., N. Rega, …, V. Barone. 2003. Energies, structures, and electronic properties of molecules in solution with the C-PCM solvation model. *J. Comput. Chem.* 24:669–681.

42. Schrödinger LLC. 2017. Small-molecule drug discovery suite. Schrödinger, LLC, New York, NY.

43. Huang, J., S. Rauscher, …, A. D. MacKerell, Jr. 2017. CHARMM36m: an improved force field for folded and intrinsically disordered proteins. *Nat. Methods.* 14:71–73.

44. Vanommeslaeghe, K., E. Hatcher, …, A. D. Mackerell, Jr. 2010. CHARMM general force field: a force field for drug-like molecules compatible with the CHARMM all-atom additive biological force fields. *J. Comput. Chem.* 31:671–690.

45. Phillips, J. C., R. Braun, …, K. Schulten. 2005. Scalable molecular dynamics with NAMD. *J. Comput. Chem.* 26:1781–1802.

46. Case, D. A., R. M. Betz, …, P. A. Kollman. 2016. AMBER. University of California, San Francisco, CA.

47. Jorgensen, W. L., J. Chandrasekhar, …, M. L. Klein. 1983. Comparison of simple potential; functions for simulating liquid water. *J. Chem. Phys.* 79:926–935.

48. Darden, T., D. York, and L. Pedersen. 1993. Particle mesh Ewald: an Nlog (N) method for Ewald sums in large systems. *J. Chem. Phys.* 98:10089–10092.

49. Humphrey, W., A. Dalke, and K. Schulten. 1996. VMD: visual molecular dynamics. *J. Mol. Graph.* 14:33–38, 27–28..

50. Frisch, M. J., G. W. Trucks, …, D. J. Fox. 2016. Gaussian 16 Revision E.01. Gaussian Inc, Wallingford, CT.

51. Goormaghtigh, E., V. Cabiaux, and J.-M. Ruysschaert. 1990. Secondary structure and dosage of soluble and membrane proteins by attenuated total reflection Fourier-transform infrared spectroscopy on hydrated films. *Eur. J. Biochem.* 193:409–420.

52. Friesner, R. A., R. B. Murphy, …, D. T. Mainz. 2006. Extra precision glide: docking and scoring incorporating a model of hydrophobic enclosure for protein-ligand complexes. *J. Med. Chem.* 49:6177–6196.

53. Chandra, B., A. Korn, …, S. Maiti. 2017. Stereoisomers probe steric zippers in amyloid-β. *J. Phys. Chem. B.* 121:1835–1842.

54. Das, A. K., A. Rawat, …, S. Maiti. 2015. An early folding contact between Phe19 and Leu34 is critical for amyloid-β oligomer toxicity. *ACS Chem. Neurosci.* 6:1290–1295.

55. Wurth, C., N. K. Guimard, and M. H. Hecht. 2002. Mutations that reduce aggregation of the Alzheimer's Aβ42 peptide: an unbiased search for the sequence determinants of Aβ amyloidogenesis. *J. Mol. Biol.* 319:1279–1290.

56. de Groot, N. S., F. X. Aviles, …, S. Ventura. 2006. Mutagenesis of the central hydrophobic cluster in Aβ42 Alzheimer's peptide. Side-chain properties correlate with aggregation propensities. *FEBS J.* 273:658–668.

57. Rodriguez, J. A., M. I. Ivanova, …, D. S. Eisenberg. 2015. Structure of the toxic core of α-synuclein from invisible crystals. *Nature.* 525:486–490.

58. Goldschmidt, L., P. K. Teng, …, D. Eisenberg. 2010. Identifying the amylome, proteins capable of forming amyloid-like fibrils. *Proc. Nat. Acad. Sci USA.* 107:3487–3492.

59. Nelson, R., M. R. Sawaya, …, D. Eisenberg. 2005. Structure of the cross-β spine of amyloid-like fibrils. *Nature.* 435:773–778.

60. Yin, X., S. Liu, …, R. Zhou. 2019. Different protonated states at the C-terminal of the amyloid-β peptide modulate the stability of S-shaped protofibril. *J. Chem. Phys.* 150:185102.

61. Petkova, A. T., Y. Ishii, …, R. Tycko. 2002. A structural model for Alzheimer's β -amyloid fibrils based on experimental constraints from solid state NMR. *Proc. Natl. Acad. Sci. USA.* 99:16742–16747.

62. Lopez del Amo, J. M., U. Fink, …, B. Reif. 2012. Structural properties of EGCG-induced, nontoxic Alzheimer's disease Aβ oligomers. *J. Mol. Biol.* 421:517–524.

63. Korn, A., S. McLennan, …, D. Huster. 2018. Amyloid β (1-40) toxicity depends on the molecular contact between phenylalanine 19 and leucine 34. *ACS Chem. Neurosci.* 9:790–799.

64. Mithu, V. S., B. Sarkar, …, P. K. Madhu. 2014. Curcumin alters the salt bridge-containing turn region in amyloid β(1-42) aggregates. *J. Biol. Chem.* 289:11122–11131.

65. Liang, C., S. N. Savinov, …, J. Chen. 2019. Modulation of amyloid-β42 conformation by small molecules through nonspecific binding. *J. Chem. Theory Comput.* 15:5169–5174.

66. Levine, Z. A., K. Teranishi, …, J.-E. Shea. 2019. The mitochondrial peptide humanin targets but does not denature amyloid oligomers in type II diabetes. *J. Am. Chem. Soc.* 141:14168–14179.

67. Wang, S.-H., F.-F. Liu, …, Y. Sun. 2010. Thermodynamic analysis of the molecular interactions between amyloid β-peptide 42 and (-)-epigallocatechin-3-gallate. *J. Phys. Chem. B.* 114:11576–11583.

68. Wang, S.-H., X.-Y. Dong, and Y. Sun. 2012. Thermodynamic analysis of the molecular interactions between amyloid β-protein fragments and (-)-epigallocatechin-3-gallate. *J. Phys. Chem. B.* 116:5803–5809.

69. Hyung, S.-J., A. S. DeToma, …, M. H. Lim. 2013. Insights into antiamyloidogenic properties of the green tea extract (-)-epigallocatechin-3-gallate toward metal-associated amyloid-β species. *Proc. Natl. Acad. Sci. USA.* 110:3743–3748.

70. Hoyer, W., C. Grönwall, …, T. Härd. 2008. Stabilization of a β-hairpin in monomeric Alzheimer's amyloid-β peptide inhibits amyloid formation. *Proc. Natl. Acad. Sci. USA.* 105:5099–5104.